Evolution of interfacial dislocation network during anisothermal high-temperature creep of a nickel-based superalloy

M. Hantcherli,[a,*] F. Pettinari-Sturmel,[a] B. Viguier,[b] J. Douin[a] and A. Coujou[a]

[a] *CEMES-CNRS, BP 94347, 29 rue Jeanne Marvig, 31055 Toulouse cedex 4, France*
[b] *Institut Carnot CIRIMAT, INP/ENSIACET – Université de Toulouse, 4 allée Emile Monso, BP 44362, 31030 Toulouse, France*

The effect of thermal cycling creep on the dislocation networks at the γ/γ' interfaces in the MC2 superalloy is investigated. Tensile creep tests were performed under thermal cycling and isothermal conditions at low stress (80 MPa) and high temperature (1150 °C). In these conditions γ' rafts may dissolve and reprecipitate during thermal cycling creep. The difference between the effects of isothermal and thermal cycling conditions on the γ/γ' interface dislocation networks, characterized by transmission electron microscopy, is exposed, as well as their evolution during the cycle.

Keywords: MC2; Single-crystal superalloy; TEM; Interfacial dislocations; Thermal cycling creep

Single-crystal nickel-based superalloys are currently used in the most advanced gas turbine engines for aircraft and helicopters. They consist of two phases: a high volume fraction of coherently precipitated γ' cubes ($L1_2$-ordered cubic phase) separated by thin channels of face-centered cubic (fcc) γ solid solution matrix. During high-temperature creep of such alloys, the γ' morphology changes from cubes to rafts [1–3], which are covered by misfit dislocation networks [4,5].

Several authors have investigated the dislocations found at the interfaces and in the γ' rafts [6–10]. It has been shown that the interfacial networks play an important role in stress accommodation and enhance the creep resistance of the superalloys [4,11]. This network, consisting of **a/2[1 1 0]** and **a[1 0 0]** dislocations, is hexagonal and regular during secondary creep [6]. However, these investigations were conducted after isothermal creep. Recent studies have shown that the thermal cycling creep rate is higher than the isothermal creep rate and that the lifetime at high temperature is shorter during non-isothermal creep [12,13].

The aim of the present work is to compare the interface dislocation networks between isothermal and thermal cycling conditions by means of interrupted creep tensile tests. The lattice mismatch parameter was also estimated through determination of the dislocation spacings.

* Corresponding author. E-mail: muriel.hantcherli@cemes.fr

The MC2 single-crystal nickel-based superalloy that was investigated was provided by Turbomeca. Its nominal weight composition is given in Table 1. It was developed by ONERA for single-crystalline turbine blades of helicopter turboshaft engines. After an appropriate heat treatment (3 h at 1300 °C/6 h at 1080 °C/20 h at 870 °C), its microstructure consists of a homogeneous distribution of strengthening cubical γ' particles (with an average edge length of 0.44 μm in the $\langle 0\,0\,1\rangle$ direction [14]) merged in an fcc γ matrix. The 70% γ' volumic fraction obtained is known to optimize the creep resistance along the [0 0 1] tension direction [15].

Crept single-crystalline samples were machined with an axis within 7° from the [0 0 1] crystallographic direction.

For reference, an isothermal creep test was performed at 1150 °C under a pressure of 80 MPa. Thermal cycling creep tests were also conducted. The anisothermal creep conditions are as follows [16]:

(i) the sample is heated from room temperature to 1150 °C in 5 min;
(ii) the sample is maintained at 1150 °C for 30 min;
(iii) the sample is cooled down to room temperature in 25 min.

To determine the effect of thermal cycling creep conditions on dislocation networks, the creep tests were interrupted at different stages of the experiment: at the end of the 11th temperature dwell and at the beginning of the 12th one.

Table 1. Nominal composition of single-crystal MC2 superalloy (wt.%).

Ni	Cr	Co	Mo	W	Al	Ti	Ta
Bal.	7.22	4.98	2.06	7.1	5.45	1.3	5.6

The different conditions are summarized in Table 2. The cooling is different for the isothermal creep and thermal cycling creep tests. In the case of the isothermal test, the sample is cooled down inside the furnace, the temperature of the sample decreasing from 1150 to 900 °C in 21 s. For thermal cycling creep tests, a quench by air cooling is performed: in this case, the temperature of the sample decreases from 1150 to 900 °C in 9.5 s so that the high-temperature microstructure is fixed.

The thin foils were prepared from specimens cut parallel to the crystallographic plane (0 0 1) and thinned by the twin jet polishing technique using the A3 Struers© electrolyte at −11 °C.

Dislocation analysis was performed in a Jeol 2010 transmission electron microscope in two beam diffraction contrast conditions. The Burgers vectors of different dislocations were determined using the standard contrast extinction rules. For each Burgers vector type, a minimum of two cases of effective invisibility were used. For each sample, different areas were examined in detail to ensure that the interfacial network observed is representative of the studied material.

Transmission electron microscopy (TEM) observations of the A12 sample, crept at 1150 °C under 80 MPa and interrupted at the beginning of the 12th temperature dwell, are shown in Figure 1, using different **g**-vectors. The dislocations observed at the interface are edge dislocations. Arrow 1 points at a dislocation with an Burgers vector. Arrow 2 points at a dislocation, which is out of contrast under the **0 2 0** reflection. The Burgers vectors of this dislocation were determined to be **a[1 0 0]**. Parallel dislocations forming a square networks are clearly identified by arrows 3 and 4. The Burgers vectors of these two types of dislocations are analyzed as being $\mathbf{a}/2[\mathbf{1}\,\mathbf{1}\,\mathbf{0}]$ and a/2[110], respectively.

In some cases, for the $\mathbf{a}\langle\mathbf{1}\,\mathbf{0}\,\mathbf{0}\rangle$ segment, the contrast observed suggests the presence of two distinct dislocation lines. For further investigations, some dark-field observations were made of this sample, and an example is shown in Figure 2. The presence of small square nodes is visible on these images. Usually the intersection between **a/2[1 1 0]** dislocations gives a **a[1 0 0]** junction (Fig. 2d), but in some cases a square composed by dislocations having $\mathbf{a}/2[\mathbf{0}\,\bar{\mathbf{1}}\,\mathbf{1}]$, **a/2[0 1 1]**, $\mathbf{a}/2[\mathbf{1}\,\mathbf{0}\,\mathbf{1}]$, **a/2[1 0 1]** Burgers vectors is observed (Fig. 2c). A model for nucleation of new square loops at [1 0 0] junction segments was proposed by Mompiou and Caillard [17].

The evolution of the interfacial γ/γ′ dislocation network was studied by comparing specimens interrupted at different stages of the thermal cycling creep with an

Table 2. Creep conditions for each sample studied.

Sample	Type	Cooling	Duration at 1150 °C
I	Isothermal	Furnace cooling	14 h
A11	Thermal cycling	Air quenching	5.5 h – end of the 11th temperature dwell
A12	Thermal cycling	Air quenching	5.5 h – beginning of the 12th temperature dwell

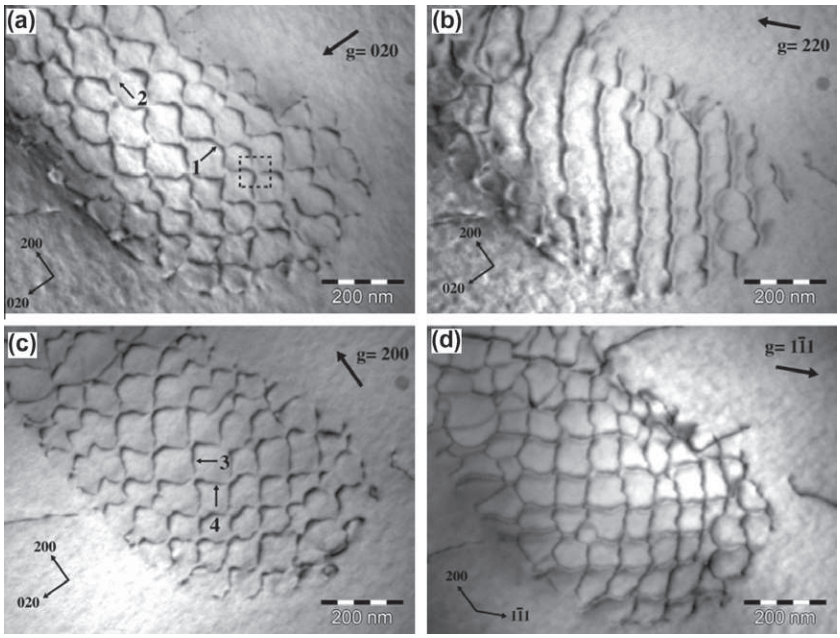

Figure 1. TEM bright-field images using different **g**-vectors of interfacial γ/γ′ dislocation networks of sample A12. The thermal cycling creep was interrupted at the beginning of the 12th temperature dwell. The foils were prepared perpendicular to the stress axis. (a) $\mathbf{g} = 020$, (b) $g = \bar{2}20$, (c) $\mathbf{g} = 200$, (d) $\mathbf{g} = 1\bar{1}1$.

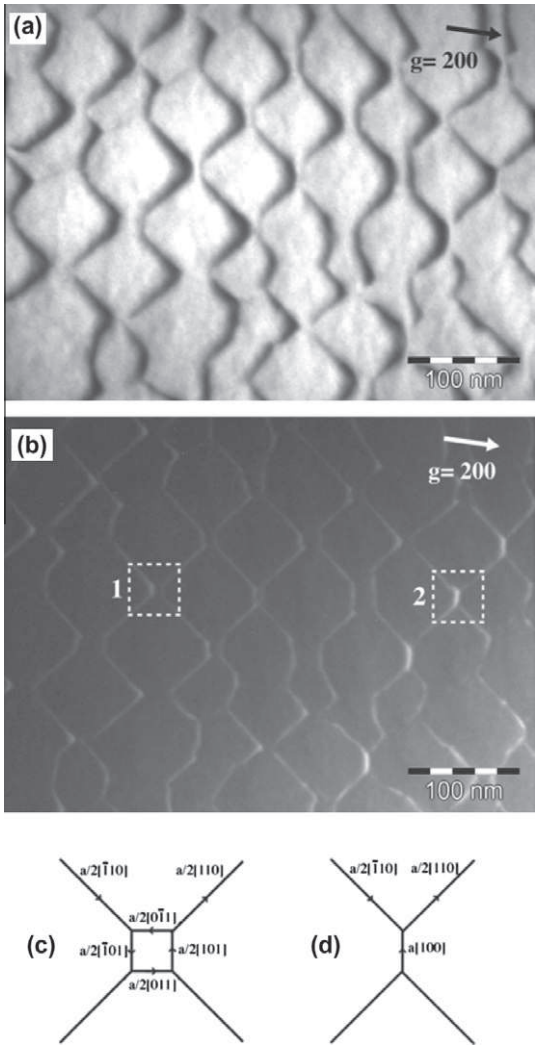

Figure 2. TEM observations of interfacial dislocation networks. The foils were prepared perpendicular to the stress axis. (a) Bright-field image with $\mathbf{g} = 200$ vector; (b) **g**–5**g** dark-field image of the same area. (c) Schematic description of the square node of interfacial networks. (d) A [100] junction.

isothermal crept sample. The dislocation network of the A12 sample has already been presented in Figure 1. For the sample crept under isothermal conditions, and for a thermal cycling creep interrupted at the end of the 11th temperature dwell, the observations are summarized in Figure 3a and b, respectively. For each studied sample, the network is regular. The dislocations, which composed the interfacial networks, were again in square configurations, and the Burgers vectors determined in each case are the same as the Burgers vectors identified in the A12 sample. Moreover, square nodes, such as the one shown in Figure 2c, were observed for each set of creep conditions. Although there were differences in the creep conditions between the different samples, the interfacial dislocation networks are similar, seem to remain quite stable and are not affected by thermal cycling.

The lattice mismatch parameters can be evaluated by the measurement of the projected dislocation spacings. In order to undertake a proper statistical analysis for a

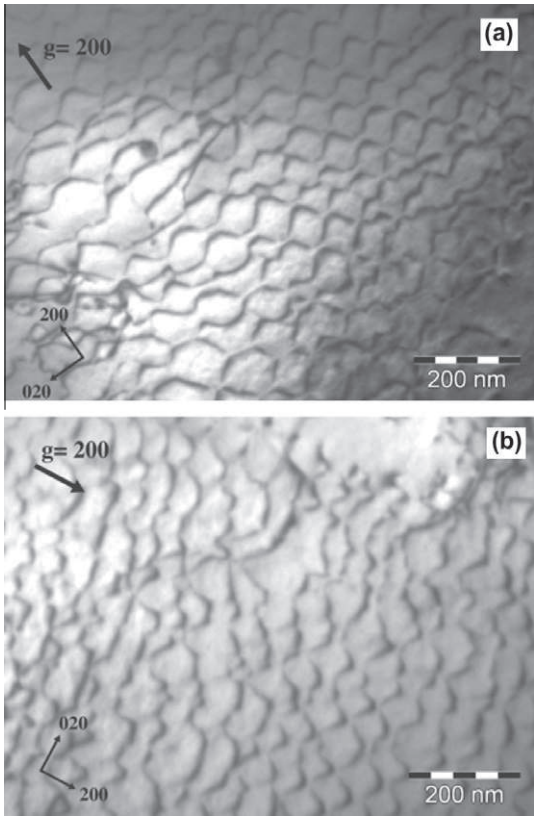

Figure 3. Interfacial dislocation networks after creep tests at 1150 °C and 80 MPa. The foils were prepared perpendicular to the stress axis. The TEM bright-field images were taken with $\mathbf{g} = 200$ vector. (a) Sample I: isothermal creep conditions; (b) sample A11: thermal cycling creep interrupted at the end of the 11th temperature dwell.

correct determination of this parameter, it is necessary to analyze a large number of dislocation spacings. In this study, between 190 and 220 measurements were considered for each sample. The results are shown in Figure 4. A similar distribution of dislocation spacings is observed for all the studied specimens. There are no visible differences between the samples crept under different conditions, and the more representative spacing observed is close to 50–55 nm in size.

The lattice mismatch parameters can be estimated by determining the average dislocation spacings. In these networks, the average dislocation spacings d is inversely proportional to the magnitude of lattice mismatch $|\delta|$ according to the following equation [6]:

$$|\delta| = b/d$$

where b is the magnitude of the **a/2[1 1 0]** Burgers vector.

The values of the lattice mismatch parameters for the I, A11 and A12 specimens are $|\delta| = 0.42\%$, $|\delta| = 0.43\%$ and $|\delta| = 0.42\%$, respectively. No significant difference is observed. Our observations are in good agreement with the results obtained by Royer et al. [18] using high-energy X-ray diffraction, showing a $|\delta|$ value between 0.48% and 0.33% during secondary creep in the AM1 superalloy.

The dislocations networks observed in each sample are similar. They have comparable characteristics and have the same morphology. The dislocations are usually

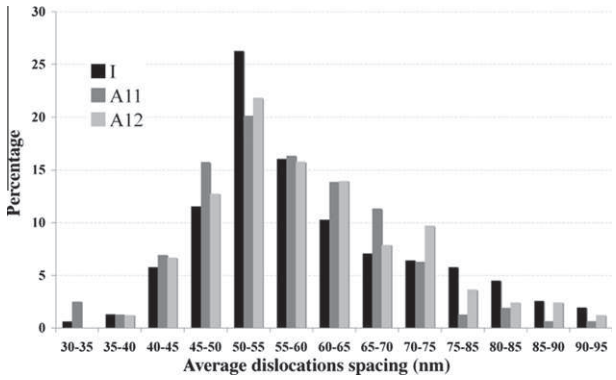

Figure 4. Average projected dislocation spacings for each sample studied. Sample I: isothermal creep conditions; sample A11: thermal cycling creep interrupted at the end of the 11th temperature dwell; sample A12: thermal cycling creep interrupted at the beginning of the 12th temperature dwell.

arranged in regular square networks, and the Burgers vectors are the same. Moreover, the spacing of dislocations, in direct relation with the lattice mismatch parameter, does not vary with the different creep conditions studied.

Nevertheless, different recent studies [12,13] have shown the dramatic effect of non-isothermal conditions on the creep properties of nickel-based superalloys at 1150 °C. The thermal cycling during creep is responsible for an important increase in the creep rate, which leads to a decrease in lifetime at high temperature. During the thermal cycling for such a temperature, the microstructure is modified by the dissolution of γ' precipitates during heating and their reprecipitation when the sample is cooled down.

During creep along the [0 0 1] load direction, the **a/2[1 1 0]** dislocations present in γ/γ' interfaces, which have a Schmidt factor equal to zero, are not activated by the load applied. These dislocations are the result of interactions between **a/2[0 1 1]** and **a/2[1 0 1]** dislocations [7]. The observation of regular interfacial networks composed of **a/2[1 1 0]** and **a[100]** dislocations, which are contained in the (0 0 1) plane, is evidence that the **a/2[0 1 1]** and **a/2[1 0 1]** dislocations have already reacted and that the γ/γ' networks obtained are stable and accommodate the misfit between the two phases. Our results for the A11 and A12 specimens show that, despite the dissolution and reprecipitation of γ' precipitates, the morphology of the interfacial networks and their stability are not affected during the thermal cycling. Moreover, the same morphology is also observed in isothermal crept sample I. From the present study, it appears that the different creep behaviors observed during thermal cycling creep as compared to isothermal creep (namely higher creep rate and shorter high-temperature lifetime [12]) are not related to differences in the γ/γ' interfacial dislocation networks.

The authors thank Turbomeca for providing specimens and the RTRA Sciences et Technologie pour l'Aéronautique et l'Espace for a post-doctoral grant (M.H.).

[1] A. Epishin, T. Link, P.D. Portella, U. Bruckner, Acta Mater. 48 (2000) 4167.
[2] J.K. Tien, S.M. Copley, Metall Trans. 2 (1971) 215.
[3] N. Matan, D. C Cox, C.M.F. Rae, R.C. Reed, Acta Mater. 47 (1999) 2031.
[4] T.M. Pollock, A.S. Argon, Acta Metall. Mater. 42 (1994) 1859.
[5] T. Sugui, Z. Huihua, Z. Jinghua, Y. Hongcai, X. Yongbo, H. Zhuangqi, Mater. Sci. Eng. A279 (2000) 160.
[6] T.P. Gabb, S.L. Draper, D.R. Hull, R.A. Mackay, M.V. Nathal, Mater. Sci. Eng. A118 (1989) 59.
[7] T. Link, A. Epishin, M. Klaus, U. Brückner, A. Reznicek, Mater. Sci. Eng. A405 (2005) 254.
[8] H. Gabrisch, D. Mukherji, Acta Mater. 48 (2000) 3157.
[9] P.M. Sarosi, R. Srinivasan, G.F. Eggeler, M.V. Nathal, M.J. Mills, Acta Mater. 55 (2007) 2509.
[10] M. Probst-Hein, A. Dlouhy, G. Eggeler, Acta Mater. 47 (1999) 2497.
[11] J.X. Zhang, T. Murakamo, H. Harada, Y. Koizumi, Scripta Mater. 48 (2003) 287.
[12] A. Raffaitin, D. Monceau, F. Crabos, E. Andrieu, F, Scripta Mater. 56 (2007) 277.
[13] J. Cormier, X. Milhet, J. Mendez, Acta Mater. 55 (2007) 6250.
[14] F. Touratier, E. Andrieu, D. Poquillon, B. Viguier, Mater. Sci. Eng. A510–511 (2009) 244.
[15] T. Murakamo, T. Kobayashi, Y. Koizumi, H. Harada, Acta Mater. 52 (2004) 3737.
[16] B. Viguier, F. Touratier, E. Andrieu, Phil Mag. (2011), accepted for publication.
[17] F. Mompiou, D. Caillard, Mater. Sci. Eng. A483–484 (2008) 143.
[18] A. Royer, A. Jacques, P. Bastie, M. Véron, Mater. Sci. Eng. A319–321 (2001) 800.